

Numerical Simulations of Aluminum Droplet Evaporation in Two Reference Frames

Soomin Lim¹, Sophie Brochu², Camila B. Cabrera³, Carlos D. Inastrilla³, Michael P. Kinzel^{1,*}

1,3 University of Central Florida, Orlando, Florida, 32828, USA.

2 Worcester Polytechnic Institute, Worcester, Massachusetts, 01609, USA.

Aluminum powder has been commonly used as the energetic material in solid propellants due to its high energy density. However, in actual combustion scenarios, not all aluminum powder is able to completely burn before reaching the nozzle, owing to the complicated physics of aluminum combustion. Due to this complexity, many studies have relied on analytic solutions instead of directly solving the Navier-Stokes equations. These earlier studies exhibit limitations, such as the inability to explain mass and heat transfer occurring at the interface or simulate 3-D fluid dynamics. In this study, the Volume of Fluid (VOF) method was employed to conduct direct numerical simulations of aluminum droplet evaporation. Subsequently, the developed model was compared and assessed against the evaporation model provided by the Lagrangian solver.

I. Introduction

Solid rockets are often used as the boosters that help give spacecrafts the thrust needed to overcome Earths gravitational pull. The high material density of the propellant allows these rockets to produce high energy per unit mass [1]. The propellant is often made of aluminum powder (Al) which is the fuel, ammonium perchlorate (AP) the oxidizer, and hydroxyl-terminated polybutadiene (HTPB) the binder that holds the fuel and oxidizer together. Aluminum is used as the fuel because it releases large amounts of energy during its oxidation process to Al₂O₃ and enhances the heat of combustion, propellant density, and combustion temperature in solid rockets motor (SRM) [1]. However, in actual combustion scenarios within SRMs, not all aluminum is able to completely burn before reaching the nozzle, owing to the complicated physics of aluminum combustion [2, 3]. This reality has spurred numerous researchers to investigate aluminum combustion, with a particular emphasis on the burning time of aluminum particles [2]. Such studies aim to elucidate the underlying mechanisms governing aluminum combustion and to enhance predictive models for the burning time of aluminum particles both within the SRM environment and for individual particles. Especially, the detailed modeling of individual particle combustion has attracted the attention for its ability to address the challenges associated with aluminum combustion.

However, these studies have predominantly employed analytical solutions based on the D² law to numerically solve the combustion of an aluminum droplet, mainly focusing on physico-chemical phenomena [3, 4]. Consequently, the attention to the combustion of an aluminum droplet has been paid mainly on the reaction mechanism between gaseous aluminum and the various oxidants [5]. Despite these advancements, the mass and heat transfer processes taking place at the aluminum interface during phase transition remain inadequately described. Particularly, to unravel the detailed surface chemistry in the future contributing to increased burning times—a key factor in the combustion process—it is essential to undertake direct numerical simulations of droplet undergoing phase transitions.

The desire to understand the droplet behavior during phase transitions can be realized through the application of the Volume of Fluid (VOF) method. This approach enables the scientist to detect any changes of topology and localize the position of interface [6]. Moreover, the VOF method offers valuable insights into the complex 3-D fluid dynamics and thermal transport processes that occur during the evaporation [7].

¹ Graduate Researcher, Mechanical and Aerospace Engineering, University of Central Florida.

² Undergraduate Researcher, Aerospace Engineering, Worcester Polytechnic Institute.

³ Undergraduate Researcher, Mechanical and Aerospace Engineering, University of Central Florida.

^{*} Associate Professor, Mechanical and Aerospace Engineering, University of Central Florida.

Most VOF studies on droplet evaporation have primarily focused on the water and, to lesser extent, other liquid droplet [8–18]. This study's application of the VOF method to an aluminum droplet introduces new possibilities for understanding the evaporation physics of solid propellants.

In this work, we employed the VOF method to conduct direct numerical simulations of aluminum droplet evaporation. This model was compared and assessed against the evaporation model provided by the Lagrangian solver, a well-established analytic solution. In our approach, the Lagrangian solver was integrated with the Eulerian approach to solve the gas phase, enabling the numerical simulation of aluminum droplets within SRM. To develop the VOFbased evaporation model, specific source terms were defined to represent the mass and heat transfer processes occurring during the phase transition of aluminum.

II. Methodology: Droplet Evaporation

A. Governing Equations

The VOF method defines the fractional volume of each phase in every cell. This fractional volume is used to distinguish between the different phases and identifying the cells at the interface. The methodology for this differentiation is as follows:

$$f_l(\mathbf{x},t) = \begin{cases} f_l = 0, & \textit{gas phase cells} \\ 0 < f_l < 1, \textit{interfacial cells} \\ f_l = 1, & \textit{liquid phase cells} \end{cases}$$
 (1)

where the volume fluid of liquid, f_l is used to represent the phases and interface. Meanwhile, f_a represents the volume fluid of gas.

The variations of phases are tracked through solving advection equations for f_l and f_g . These immiscible advections equations are given as

$$\frac{\partial f_l}{\partial t} + \nabla \cdot (f_l \mathbf{u}) = \frac{S_{evap}}{\rho_l}$$

$$\frac{\partial f_g}{\partial t} + \nabla \cdot (f_g \mathbf{u}) = -\frac{S_{evap}}{\rho_g}.$$
(2)

Here S_{evap} is defined by the mass transfer occurring due to evaporation at the interface. This term functions as either a sink or source term for each phase. It represents the mass traversing the interface from one phase to another and operates solely at the interfacial cells. The source term of the advection equation is defined by

$$S_{evap} = m''_{evap} \times \alpha \tag{3}$$

where α is the interfacial area density. The evaporation flux, m''_{evap} , is obtained through Fick's law and the Stefan flow, which yields [16, 19]

$$m_{evap}^{"} = \frac{\rho_g D_g (\partial Y_{Al} / \partial \mathbf{x})_{surf}}{1 - Y_{Al \ saf}}.$$
 (4)

 $m_{evap}^{\prime\prime} = \frac{\rho_g D_g (\partial Y_{Al}/\partial \mathbf{x})_{surf}}{1 - Y_{Al,sat}}.$ Here, Y_{Al} is the mass fraction of aluminum droplet and $Y_{Al,sat}$ the saturated value at the reference pressure. The gaseous diffusion coefficient, D_g , is computed through a dilute approximation provided as follow [20] $D_g = \frac{{}^{1-X_{Al,g}}}{\sum_{i,j \neq Al} (X_i/D_{i,g})}$

$$D_g = \frac{1 - X_{Al,g}}{\sum_{i,j \neq Al} (X_i/D_{i,g})}$$
 (5)

where X_i is the gaseous mole fraction of i^{th} species. The main driving force of evaporation is the mass fraction gradient at the interface, $(\partial Y_{Al}/\partial \mathbf{x})_{surf}$. The mass fraction of interfacial cells is assumed to be the saturated value due to the equilibrium state of evaporation. The mass fraction gradient is given by:

$$\left(\frac{\partial Y_{Al}}{\partial \mathbf{x}}\right)_{surf} = (\nabla Y)_{surf} \cdot \vec{n} \tag{6}$$

where \vec{n} is the normal vector to the interface pointing outward from the liquid into the gas as follows $\vec{n} = -\frac{\nabla f_l}{|\nabla f_l|}.$

$$\vec{n} = -\frac{\nabla f_l}{|\nabla f_l|}.\tag{7}$$

In this work, Y_{Al} is coupled with the temperature to account for the effects of evaporative cooling. Consequently, a temperature drop around the droplet can lead to a decrease in Y_{Al}. The Clausius-Clapeyron equation is utilized to depict the variation of aluminum mass fraction due to the change of the temperature [21]:

$$Y_{Al} = \frac{X_{Al}MW_{Al}}{X_{Al}MW_{Al} + X_{OX}MW_{OX}}$$

$$X_{Al} = \exp\left(\frac{L}{R}\left(\frac{1}{T_{Al}} - \frac{1}{T_{O}}\right)\right)$$
(8)

with MW molecular weight, L the latent heat of vaporization and subscript OX oxidant. The species and momentum equation are given by

$$\rho_m \frac{(\partial Y_i)}{\partial t} + \rho_m \mathbf{u} \cdot \nabla Y_i = \nabla \cdot (\rho_m D \nabla Y_i)$$
(9)

$$\frac{\partial(\rho_m \mathbf{u})}{\partial t} + \nabla \cdot (\rho_m \mathbf{u} \otimes \mathbf{u}) = -\nabla \mathbf{p} + \nabla \cdot [\mu_m (\nabla \mathbf{u} + (\nabla \mathbf{u})^{\mathrm{T}}] + \rho_m \mathbf{g} + \mathbf{f}_{\sigma}. \tag{10}$$

Note that the species source term of aluminum by the evaporation was not defined in this study. The density and viscosity of (9) and (10) are the mixture density based on the volume averaged value,

$$\rho_m = \rho_l f_l + \rho_g (1 - f_l)
\mu_m = \mu_l f_l + \mu_g (1 - f_l).$$
(11)

The energy equation is written as the enthalpy form:

$$\frac{\partial(\rho_m c_{p,m} T_m)}{\partial t} + \nabla \cdot \left(\rho_m C_{p,m} \mathbf{u} T_m\right) = \nabla \cdot (\lambda \nabla T_m) - L \times S_{evap}$$
(12)

where the viscous dissipation term is neglected. It is important to note that the energy equation incorporates a source term, $L \times S_{evap}$, to represent the thermal balance at the interface. This interfacial thermal balance is expressed by the enthalpy difference between each phase. In the evaporation case, this variation equates to the latent heat of vaporization per unit volume and thus, the source term appears with the latent heat of vaporization, L. The mixture specific heat and mixture temperature in (12) are computed by the mass averaged value,

Computed by the mass averaged value,
$$C_{p,m} = \frac{f_1 \rho_1 C_{p,l} + f_g \rho_g C_{p,g}}{f_1 \rho_1 + f_g \rho_g T_g}$$

$$T_m = \frac{f_1 \rho_1 T_1 + f_g \rho_g T_g}{f_1 \rho_1 + f_g \rho_g}.$$
(13)

B. Numerical Setup

The governing equations were solved through the segregated solve with the implicit unsteady. The interface is reconstructed based on the High-Resolution Interface Capturing (HRIC) scheme. The equivalent diameter of droplet change is calculated by the following formula:

$$d_p = \sqrt[3]{\sum V_{cell} \times \frac{3}{4} \times \frac{6}{\pi}} \tag{14}$$

The computational domain was described by two dimensional axisymmetric and the meshing for the flow field and the droplet is shown in Figure 1. The domain has 1 mm of width and 0.5 mm of height. The temperature and pressure of the gas domain were set to the boiling temperature of aluminum droplet, that is 2790 K and 1 bar, respectively. The diameter of the droplet is consistent with the diameter of the aluminum droplet as specified in the Eulerian-Lagrangian approach.

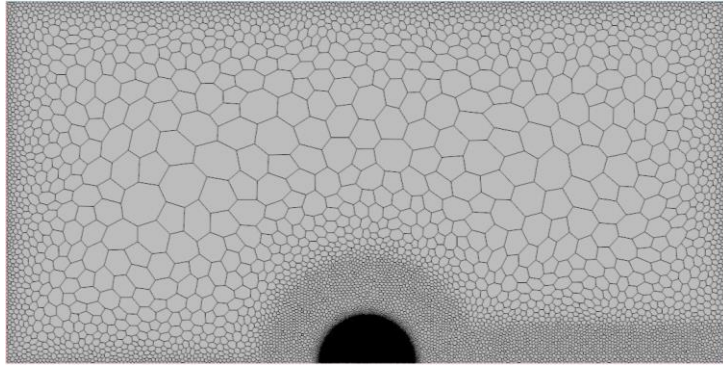


Fig. 1 2D axisymmetric flow field around the droplet with mesh grids.

III. Methodology: Solid Rocket Motor

A. Eulerian Phase

The continuum part of the solid rocket motor was described by the Eulerian approach and the governing equations were solved through the Reynolds-averaged Navier-Stokes (RANS) turbulence model. The k- ω SST model was employed for the turbulence modeling. Additionally, the chemical reactions of evaporated aluminum were incorporated into the model. Consequently, gaseous aluminum was considered to dissipate post-evaporation. The specific chemical reactions accounted for in this study are shown in Table 1.

Table 1 Input chemical reactions.

Chemical reactions	
$Al_{(g)} + O_2 \rightarrow AlO + O$	
$AlO + O_2 \rightarrow AlO_2 + O$	
$AlO + CO_2 \rightarrow AlO + CO$	
$Al + H_2O \rightarrow AlO + H_2$	
$O + O + M = O_2 + M$	
$O + N_2 \rightarrow NO + N$	

B. Lagrangian Model

The aluminum droplets were treated as non-continuum and their motions were computed through the Lagrangian Solver. Newton's law of motion was employed to describe the forces acting on the droplets and the properties of the discrete phase were updated along the parcel streamline. Since the main interest of the Lagrangian solver is to compute the evaporation time of aluminum droplet, we focus on the evaporation rate of the Lagrangian solver.

Aluminum evaporation is supposed to follow a classical D^2 law and the quasi-steady evaporation model [3, 22]. This model conceptualizes droplet evaporation as being governed by heat transfer limitation, which is outlined as follows:

$$\dot{m}_p = -g^* A_s \ln(1+B) \tag{15}$$

where g^* is the mass transfer conductance, A_s the particle surface area, B the Spalding transfer number. The Spalding transfer number is given by

$$B = \frac{c_p(T - T_p)}{L} \tag{16}$$

and the mass transfer conductance

$$g^* = \frac{k \operatorname{Nu}_p}{C_p D_p} \tag{17}$$

where Nusselt number is calculated through the Ranz-Marshall correlation,

$$Nu_p = 2(1 + 0.3Re_p^{1/2}Pr^{1/3}). (18)$$

Note that the subscript p represents the particle.

C. Geometry and Boundary Conditions

The geometry of the nozzle was generated by inserting and tracing nozzle provided by Ramsey *et al.*, on SolidWorks using the sketch picture tool [23]. The nozzle was then imported into StarCCM+ where a mesh was created as seen in Figure 2. The aluminum droplets are injected into the chamber through the part injector. The detailed boundary conditions for the chamber and injector are shown in Table 2.

Pressure outlets: extrapolated backflow

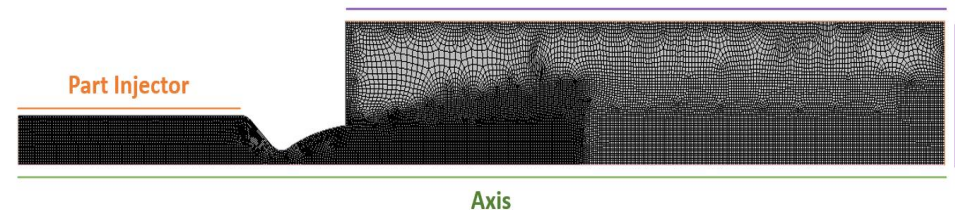


Fig. 2 Mesh and boundary conditions.

Table 2 Summary of boundary conditions of chamber and injector.

Properties	Value
Chamber temperature	2800 K
Chamber pressure	1.5 bar
Mach number	0.052
Particle flow rate (Injector)	5.0 /s
Particle temperature	2790 K
Particle velocity	1.0 m/s

IV. Results and Discussion

In this section, the evaporation of aluminum droplet is numerically simulated using the two distinct methodologies: that is the Lagrangian solver and the VOF approach. The evaporation time of the aluminum droplet is evaluated using both methods. Furthermore, the evaporation model of aluminum droplet using the VOF method is assessed by comparing the evaporation times obtained from the Lagrangian solver and by estimating its capability in phase tracking.

A. Lagrangian Approach

The numerical modeling of the SRM incorporating aluminum particles was conducted. Figures 3 and 4 illustrate the outcomes obtained through the Eulerian-Lagrangian approach for the SRM with aluminum particles. As expected, the contour of temperature and pressure showed the decreasing behavior from the nozzle's throat. However, an atypical rise in pressure and temperature was observed in the mid-region of the diverging section, varying from the conventional relationship between the converging-diverging nozzle and the fluids properties. The Mach number and velocity exhibited an inverse relationship to the temperature and pressure, as shown in Figure 4.

The unusual trend in fluid's properties occurring at the nozzle might stem from the negative pressure values at the observed in nozzle, coupled with the significantly low pressure in the chamber. For the purpose of this study, however, the pressure was set to 1.5 bar to facilitate a comparison of evaporation times using the VOF model. It's important to note that the current VOF model does not accommodate the actual high combustion pressure. As a result, while the observed trends in combustion gas properties from the nozzle's throat deviate from previous studies, the SRM combustion model used here is still effective for calculating fluid properties inside the chamber and the evaporation time of aluminum droplets. Therefore, the decision was made to use only the results from within the chamber, excluding the nozzle portion, for comparing evaporation times.

In contrast, our previous study demonstrated the validity of the Eulerian-Lagrangian approach in modeling SRM with aluminum particles when a high-pressure inlet is applied. Consequently, this model will serve as a benchmark for evaporation time and will provide varying boundary conditions of aluminum droplet—such as those in the chamber, converging section, and diverging section—to assess the evaporation time in the VOF-based model.

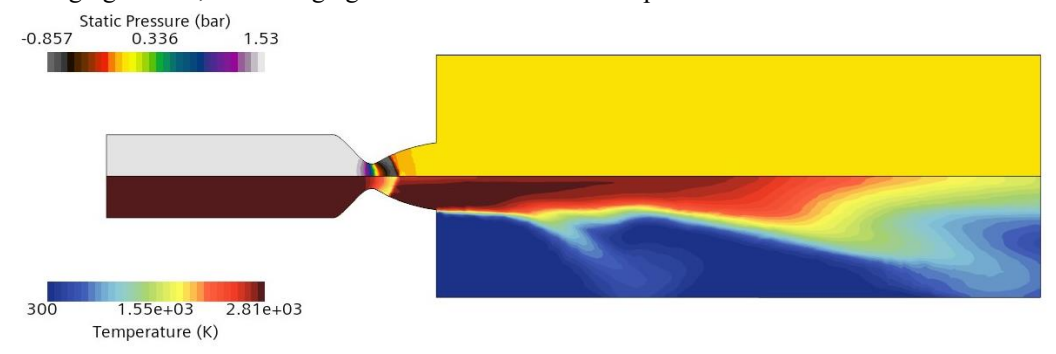


Fig. 3 Pressure and temperature contour of SRM.

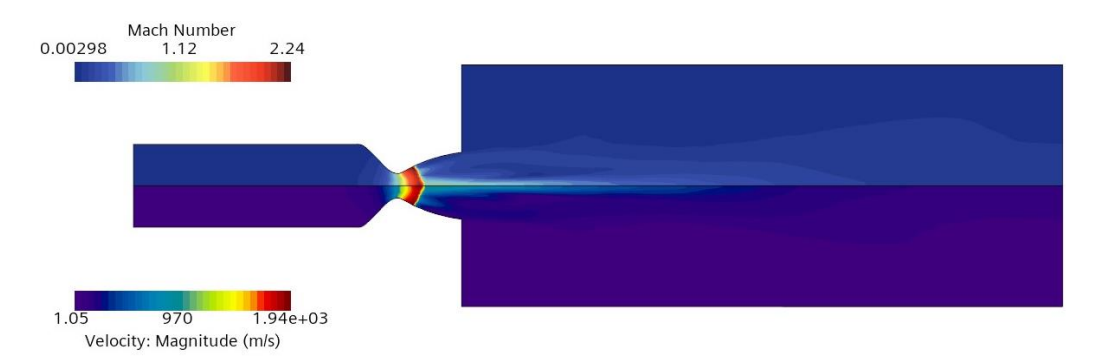


Fig. 4 Mach number and velocity contour of SRM.

As previously discussed, the parcels of particular interest in this study are those that flow within the chamber, exhibiting boiling temperature of aluminum at 1.5 bar. Figure 5 highlights the selection of a specific parcel, which traverses the chamber within the solution time, from the overall parcel streamline. For in-depth analysis, parcel with indices 48 and 203 were specifically chosen.

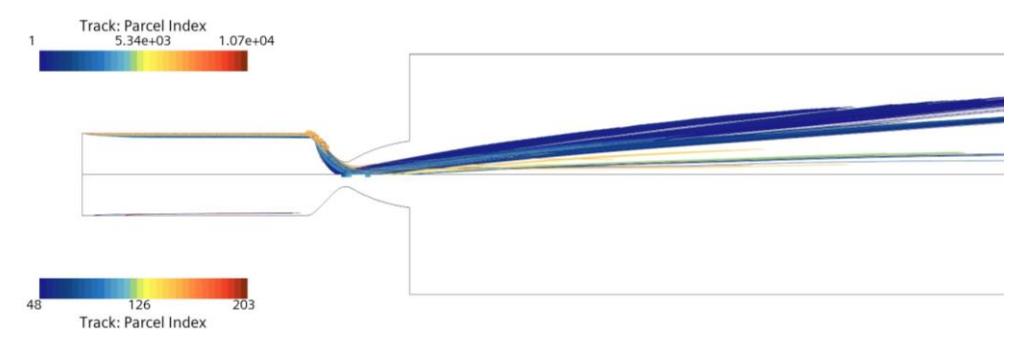


Fig. 5 Comprehensive overview of parcel streamlines (upper) and individual parcel (lower).

Figure 6 shows the time-dependent changes in the diameter of an aluminum droplet associated with an individual parcel. The evaporation rate is notably slow as depicted in Figure 6. Specifically, for parcel 48, the diameter exhibits a reduction of $0.0137 \, \mu m$ for 5 ms. These temporal diameter variations will be used for comparing the evaporation rate obtained from the VOF-based model.

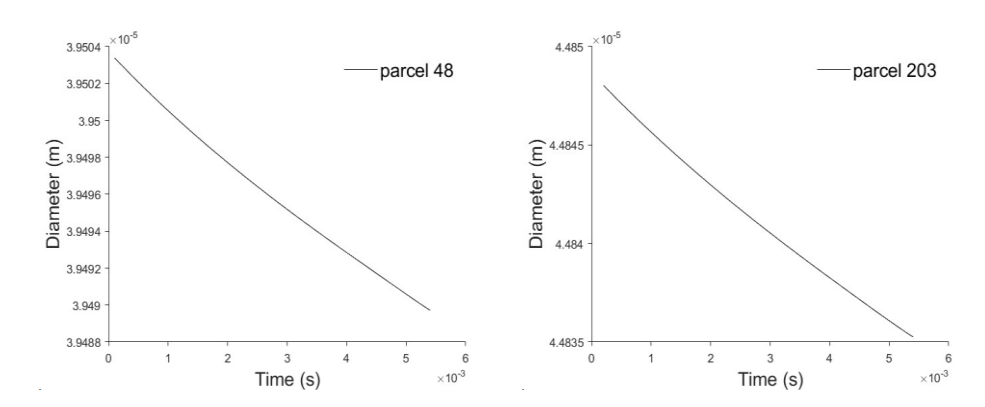


Fig. 6 Temporal variation in the diameter of an aluminum droplet in an individual parcel.

B. VOF Method

In this section, the evaporation model of a single aluminum droplet based on the VOF method is described. Given the same velocity of the injected droplets and gaseous velocity within the chamber of SRM, the gas domain in the VOF model was considered non-convective system. Two droplets were modeled, each possessing the same diameter

as an individual parcel modeled in the Lagrangian approach, to facilitate a comparative analysis of evaporation times across two reference frames.

Figure 7 displays the time-dependent changes of the parcel 48 and 203, as modeled using the VOF approach. It is observed that the droplet with a larger diameter exhibits a longer evaporation time aligning with expectations. However, it is notable that the evaporation time calculated the VOF method is significantly shorter than that derived from the Lagrangian approach.

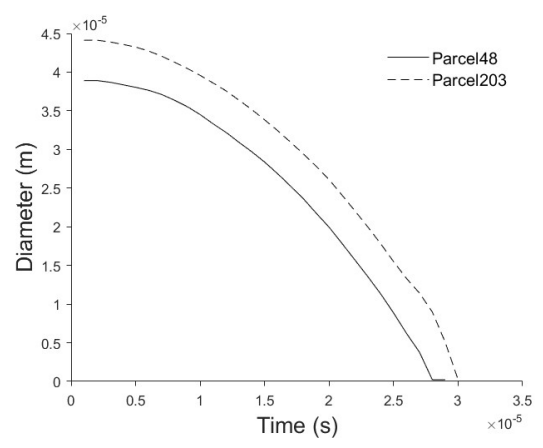


Fig. 7 Diameter changes of a single aluminum droplet as a function of time based on the VOF method.

This substantial discrepancy may arise from issues related to mass conservation in the application of the VOF method in this study. Figure 8 indicates that the total aluminum mass variation of parcel 48 within the entire computational domain is not conserved throughout the evaporation process.

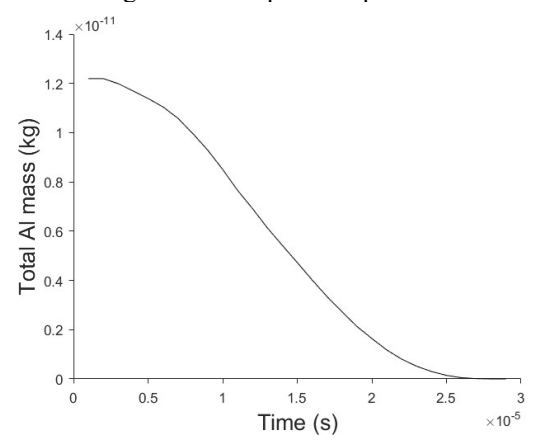


Fig. 8 Total aluminum mass within the computational domain during the evaporation process.

Although there is a notable discrepancy in the evaporation time modeled through the VOF method compared to the Lagrangian approach, the VOF method successfully captures the droplet's shape change and the temperature variations resulting from evaporative cooling, as achieved through the implementation of source terms. Figure 9 visually shows these shape changes in the droplet, along with the temperature variations surrounding it and the aluminum fraction changes due to the temperature reduction. This implies coupling the aluminum mass fraction with the temperature was successfully imported into the model. Meanwhile, it is observed that the local temperature decreases to 2710 K, followed by a subsequent increase attributed to the heat conduction from the surrounding gases at a higher temperature.

This research defines the source terms of governing equations of the VOF approach to track the interface change and temperature variations due to phase transition. Many studies on the droplet evaporation using the VOF method have employed Fick's law as their source term of the advection equation as described in the preceding section of this research [7–9, 24, 25]. However, our findings suggest that the mere application of Fick's law does not ensure the mass conservation across the entire computational domain. This implies the necessity for additional research on the VOF-simulated droplet evaporation.

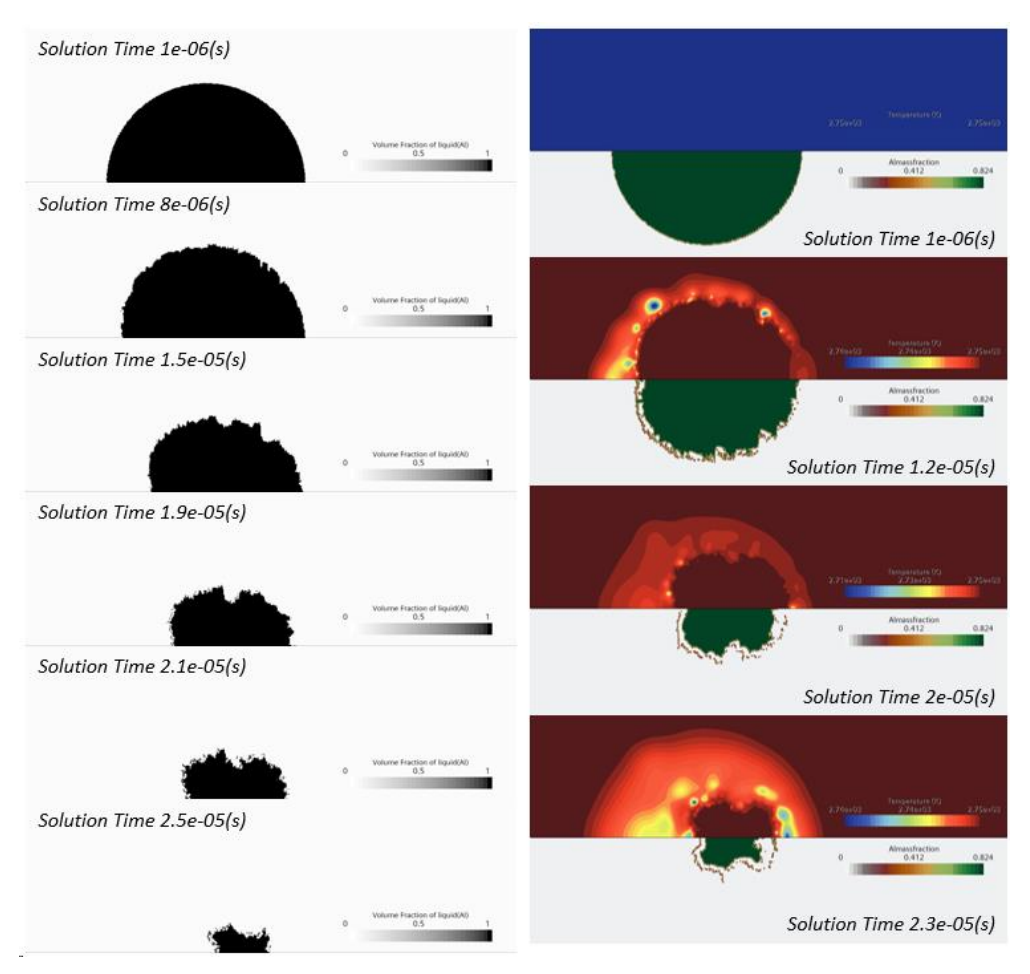


Fig. 9 Time-dependent changes of the droplet shape (left) and temperature and aluminum mass fraction (right)

V. Conclusion

The numerical simulation of aluminum droplet evaporation within the SRM was accomplished using two distinct methods. The Eulerian-Lagrangian approach was employed to capture the behavior of the aluminum droplet within the SRM, with the Lagrangian solver predicting its trajectory and the gas domain being characterized using the RANS turbulence model. The droplet evaporation was governed by heat transfer limited evaporation model based on the quasi-steady state. The aluminum droplets were injected into the combustion chamber with the injector velocity 1.0 m/s and droplet temperature 2790 K. Two individual parcels from all parcels were selected to specifically investigate the evaporation time of the aluminum droplet. The observed evaporation rate showed the reduction of $0.0137 \, \mu \text{m}$ in the diameter of the parcel $48 \, \text{d} \text{u} \text{ring} \, 5 \, \text{ms}$.

In the VOF method, the source terms for the advection equation and the energy equation were defined to model the evaporation of a single aluminum droplet. The advection source terms were derived from Fick's law, while the energy source term was defined based on the enthalpy difference between each phase. Notably, the evaporation time from the VOF method indicated a more rapid evaporation time of aluminum droplet as compared to results from the Lagrangian solver, highlighting a significant variance. Concurrently, it was observed that the total aluminum mass of the droplet within the computational domain was not conserved. The discrepancy of the evaporation time may arise from this mass conservation issue. Despite this, the VOF model of this study proficiently represented the morphological evolution of the droplet and the decrease in both temperature and aluminum mass fraction resulting from evaporative cooling. These dynamics were effectively delineated through the implementation of the source terms.

Along with the discrepancies in evaporation time between the two reference frames and the mass conservation issue of the VOF method, the omission of certain source terms indicates the need for further research on aluminum droplet evaporation to accurately track the phase changes. For example, defining a species source term of the fuel

droplet could significantly influence not only the species equation, but also other governing equations. This is due to the fact that the production of gaseous aluminum would alter the volume fraction adjacent the interface, leading to the inaccuracies in modeling. These inaccuracies stem from shifts in fluids material properties that involve the volume fraction, *e.g.*, properties of mass-averaged and volume-averaged. Therefore, detailed research on the droplet evaporation of aluminum using the VOF method is imperative.

References

- [1] S. Chaturvedi and P. N. Dave, "Solid propellants: AP/HTPB composite propellants," *Arabian Journal of Chemistry*, vol. 12, no. 8, pp. 2061–2068, Dec. 2019, doi: 10.1016/j.arabjc.2014.12.033.
- [2] J. Glorian, S. Gallier, and L. Catoire, "On the role of heterogeneous reactions in aluminum combustion," *Combust Flame*, vol. 168, pp. 378–392, Jun. 2016, doi: 10.1016/j.combustflame.2016.01.022.
- [3] M. Beckstead, "A Summary of Aluminum Combustion," 2002. [Online]. Available: https://www.researchgate.net/publication/216833898
- [4] M. Mathieu, D. Dmitry, and G. Vincent, "Computational study of Al droplet combustion in a burning solid propellant environment," 2019, doi: 10.13009/EUCASS2019-202.
- [5] J. H. Wang, J. Luo, S. X. Huang, J. Xia, B. Yang, and Y. Wang, "Numerical simulation of single aluminum droplet evaporation based on VOF method," *Case Studies in Thermal Engineering*, vol. 34, Jun. 2022, doi: 10.1016/j.csite.2022.102008.
- [6] J. Schlottke and B. Weigand, "Direct numerical simulation of evaporating droplets," *J Comput Phys*, vol. 227, no. 10, pp. 5215–5237, May 2008, doi: 10.1016/j.jcp.2008.01.042.
- [7] G. Strotos, I. Malgarinos, N. Nikolopoulos, and M. Gavaises, "Predicting the evaporation rate of stationary droplets with the VOF methodology for a wide range of ambient temperature conditions," *International Journal of Thermal Sciences*, vol. 109, pp. 253–262, Nov. 2016, doi: 10.1016/j.ijthermalsci.2016.06.022.
- [8] J. Reutzsch, C. Kieffer-Roth, and B. Weigand, "A consistent method for direct numerical simulation of droplet evaporation," *J Comput Phys*, vol. 413, Jul. 2020, doi: 10.1016/j.jcp.2020.109455.
- [9] K. Eisenschmidt *et al.*, "Direct numerical simulations for multiphase flows: An overview of the multiphase code FS3D," *Appl Math Comput*, vol. 272, pp. 508–517, Jan. 2016, doi: 10.1016/j.amc.2015.05.095.
- [10] J. H. Wang, J. Luo, S. X. Huang, J. Xia, B. Yang, and Y. Wang, "Numerical simulation of single aluminum droplet evaporation based on VOF method," *Case Studies in Thermal Engineering*, vol. 34, Jun. 2022, doi: 10.1016/j.csite.2022.102008.
- [11] C. Ma and D. Bothe, "Numerical modeling of thermocapillary two-phase flows with evaporation using a two-scalar approach for heat transfer," *J Comput Phys*, vol. 233, pp. 552–573, Jan. 2013, doi: 10.1016/j.jcp.2012.09.011.
- [12] J. Reutzsch, C. Kieffer-Roth, and B. Weigand, "A consistent method for direct numerical simulation of droplet evaporation," *J Comput Phys*, vol. 413, Jul. 2020, doi: 10.1016/j.jcp.2020.109455.
- [13] S. Hardt and F. Wondra, "Evaporation model for interfacial flows based on a continuum-field representation of the source terms," *J Comput Phys*, vol. 227, no. 11, pp. 5871–5895, May 2008, doi: 10.1016/j.jcp.2008.02.020.
- [14] L. Malan, "Direct numerical simulation of free-surface and interfacial flow using the VOF method: cavitating bubble clouds and phase change," University of Cape Town, 2017. [Online]. Available: https://theses.hal.science/tel-01875719
- [15] Tryggvason, Gre, tar, Zaleski, Scardovelli, and Ruben, *Direct Numerical Simulations of Gas-Liquid Multiphase Flows*. Cambridge University Press, 2011.
- [16] G. Strotos, I. Malgarinos, N. Nikolopoulos, and M. Gavaises, "Predicting the evaporation rate of stationary droplets with the VOF methodology for a wide range of ambient temperature conditions," *International Journal of Thermal Sciences*, vol. 109, pp. 253–262, Nov. 2016, doi: 10.1016/j.ijthermalsci.2016.06.022.
- [17] J. Schlottke and B. Weigand, "Direct numerical simulation of evaporating droplets," *J Comput Phys*, vol. 227, no. 10, pp. 5215–5237, May 2008, doi: 10.1016/j.jcp.2008.01.042.
- [18] K. Eisenschmidt *et al.*, "Direct numerical simulations for multiphase flows: An overview of the multiphase code FS3D," *Appl Math Comput*, vol. 272, pp. 508–517, Jan. 2016, doi: 10.1016/j.amc.2015.05.095.
- [19] L. Zhou, Theory and Modeling of Dispersed Multiphase Turbulent Reacting Flows. Butterworth-Heinemann, 2018.
- [20] R. B. Bird, W. E. Steward, and E. N. Lightfoot, *Transport Phenomena*, 2nd ed. New York: John Wiley & Sons, Inc., 2002.

- [21] K. K. Kuo, *Principles of Combustion*, 2nd ed. New Jersey: John Wiley & Sons, Inc.
- [22] S. Gallier and F. Godfroy, "Aluminum combustion driven instabilities in solid rocket motors," *J Propuls Power*, vol. 25, no. 2, pp. 509–521, 2009, doi: 10.2514/1.37664.
- [23] M. C. Ramsey, R. W. Pitz, T. P. Jenkins, Y. Matsutomi, C. Yoon, and W. E. Anderson, "Planar 2D velocity measurements in the cap shock pattern of a thrust optimized rocket nozzle," *Shock Waves*, vol. 22, no. 1, pp. 39–46, Jan. 2012, doi: 10.1007/s00193-011-0340-0.
- [24] C. Ma and D. Bothe, "Numerical modeling of thermocapillary two-phase flows with evaporation using a two-scalar approach for heat transfer," *J Comput Phys*, vol. 233, pp. 552–573, Jan. 2013, doi: 10.1016/j.jcp.2012.09.011.
- [25] J. Schlottke and B. Weigand, "Direct numerical simulation of evaporating droplets," *J Comput Phys*, vol. 227, no. 10, pp. 5215–5237, May 2008, doi: 10.1016/j.jcp.2008.01.042.